Available online at www.sciencedirect.com

ScienceDirect

Ceramics International 40 (2014) 1627–1633

CERAMICS INTERNATIONAL

www.elsevier.com/locate/ceramint

# Surface morphology and photoelectric properties of fluorine-doped tin oxide thin films irradiated with 532 nm nanosecond laser

Bao-jia Li[a,b,*], Li-jing Huang[a,b], Ming Zhou[c], Nai-fei Ren[b,d], Bo Wu[b,d]

[a]School of Materials Science and Engineering, Jiangsu University, Zhenjiang 212013, PR China
[b]Jiangsu Provincial Key Laboratory of Center for Photon Manufacturing Science and Technology, Jiangsu University, Zhenjiang 212013, PR China
[c]The State Key Laboratory of Tribology, Tsinghua University, Beijing 100084, PR China
[d]School of Mechanical Engineering, Jiangsu University, Zhenjiang 212013, PR China

Received 23 May 2013; received in revised form 30 June 2013; accepted 10 July 2013
Available online 24 July 2013

## Abstract

In order to improve the transparency and conductivity of the commercial fluorine-doped tin oxide (FTO) films deposited on glass substrates, a nanosecond pulsed laser with a wavelength of 532 nm was used to irradiate the surfaces of the films. The effects of laser fluence and scanning speed on the surface morphology, photoelectric property and overall quality of the FTO films were investigated. The FTO films which were subjected to lower laser fluences or higher scanning speeds achieved gentle laser annealing effects, resulting in unapparent changes in surface morphology. These changes caused enhancements in optical transmittance and decrease in sheet resistance. The FTO films irradiated with higher laser fluences or lower scanning speeds melted and ablated, causing the optical transmittance and the electrical conductivity of the films to drop significantly. Experimental results indicated that the optimum irradiation fluence and scanning speed for 532 nm nanosecond laser annealing of FTO films were 1.02 J/ $cm^2$ and 10 mm/ s, respectively. The corresponding film had an obvious increase in crystallite size. The RMS roughness, the average optical transmittance in the waveband of 380–780 nm and the figure of merit were increased from 100.5 nm, 75.4% and $5.82\times10^{-3}\ \Omega^{-1}$ to 113.0 nm, 82.7% and $17.00\times10^{-3}\ \Omega^{-1}$ respectively, while the sheet resistance was reduced from 10.2 Ω/□ to 8.8 Ω/□.


*Keywords:* Fluorine-doped tin oxide (FTO); Nanosecond laser; Annealing; Surface morphology; Photoelectric property

## 1. Introduction

Transparent conductive oxide (TCO) films with high transmittance and low resistivity are in demand in many optoelectronic devices such as solar cells [1–3], flat panel displays [4], touch panels [5], light-emitting diodes (LEDs) [6], and gas sensors [7]. Among the TCO films, tin-doped indium oxide (ITO) film has been widely used for many years. However, due to the expensive and toxic indium, developing cheap and high performance TCO films is more desired. Fluorine-doped tin oxide (FTO) thin film is the TCO film of choice because it is cheap (containing no expensive indium element), and has good thermal stability as well as high chemical stability [8]. It is not enough to control the surface morphologies and photoelectric properties of FTO films by only depositing methods (such as sputtering [9], spray pyrolysis [10] and chemical vapor deposition [11,12]), so some post-anneal processes have to be employed [13]. The traditional thermal annealing processes require a high temperature (always higher than 500 °C) and a long operating period (several hours due to the electric resistance heating method). In contrast, the laser annealing process provides a way to achieve local annealing of the film without causing damage to the substrate and shorten the operating time, which can improve work efficiency and avoid escape of doping elements in the film. Moreover, during laser annealing the temperature from the surface of the film to the substrate presents a gradient distribution that can restrain diffusion of impurities from the substrate [14]. Although, a lot of research has been done on post-annealing treatment of zinc oxide (ZnO) films [15–17], aluminum-doped ZnO (AZO) films [18–20], ITO films [21,22] and $TiO_2$ films [23] using

*Corresponding author at: School of Materials Science and Engineering, Jiangsu University, Zhenjiang 212013, PR China. Tel.: +86 511 88790390; fax: +86 511 8879 1288.
*E-mail address:* bjia_li@126.com (B.-j. Li).

0272-8842/$ - see front matter © 2013 Elsevier Ltd and Techna Group S.r.l. All rights reserved.
http://dx.doi.org/10.1016/j.ceramint.2013.07.053

excimer or nanosecond lasers, the laser anneal treatments of FTO films have rarely been studied except by [24,25]. Chen et al. [24] adopted a nanosecond pulsed Nd:YAG laser with a wavelength of 1064 nm to anneal FTO films prepared by the spray pyrolysis method. After the laser annealing process, the average optical transmittance between 400 and 800 nm was slightly reduced from 80.90% to 75.30% and the sheet resistance was reduced from $639.7 \pm 40.02\ \Omega/\square$ to $595.1 \pm 29.0\ \Omega/\square$. Tseng et al. [25] utilized a nanosecond pulsed Nd:$YVO_4$ laser with a wavelength of 355 nm to anneal FTO films deposited on soda-lime glass substrates by the sputtering method. The value of the average optical transmittance for laser annealed FTO films increased approximately by 4% and all the sheet resistance of laser annealed FTO films decreased significantly compared with unannealed FTO films. The works mentioned above indicate a potential developing space for the optimization of FTO films by employing the laser anneal process. In this study, commercial FTO films deposited on glass substrates were irradiated with a nanosecond pulsed laser with a wavelength of 532 nm which was different from the wavelength adopted in the above researches. The effects of laser fluence and scanning speed on the surface morphologies and photoelectric properties of the films were systematically investigated, so as to ascertain the optimum laser parameters for improving the performance of the FTO films.

## 2. Experiment

### 2.1. Sample preparation and characterization

The commercial FTO films used in this experiment were deposited on 3.0 mm-thick plate glass substrates (expressed as FTO/glass samples) by the chemical vapor deposition method. The FTO/glass samples were cut into small pieces (15 mm × 15 mm). Before the laser irradiation, all samples were cleaned with deionized water, anhydrous ethanol and acetone in an ultrasonic bath each for 10 min and then air-dried by high-purity (99.99%) nitrogen gas. The crystal structures of the films were examined with an X-ray diffractometer (XRD) (Rigaku Corp., Japan, D/max2500VB3+/PC) with Cu-Kα radiation ($\lambda = 0.1541$ nm). The thicknesses and micromorphologies of the films were observed with a scanning electron microscope (SEM) (Carl Zeiss Inc., Germany, EVO MA10). The thickness of the FTO layer was approximately 726 nm, as measured from the SEM cross-sectional view of the FTO/glass sample shown in Fig. 1. The 3D images with the root mean square (RMS) roughnesses of the FTO films were scanned with an atomic force microscope (AFM) (Asylum Research Inc., USA, MFP-3D-SA), and the scanned surface region was 20 μm × 20 μm. The optical properties and sheet resistance of the films were tested with a spectrophotometer (Shimadzu Corp., Japan, UV-2550) and a digital four-point probe instrument (Suzhou Baishen Technology Co. Ltd., China, SX1944), respectively. Table 1 presents the measured thickness, surface RMS roughness and photoelectric properties for the FTO/glass sample.

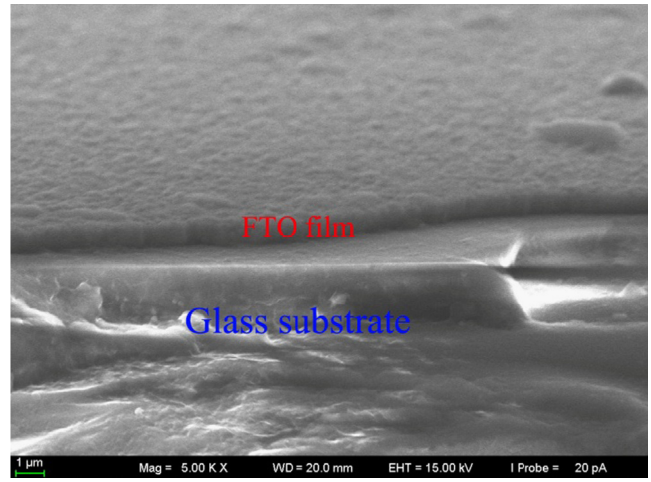

Fig. 1. A SEM cross-sectional view of the FTO/glass sample.

Table 1
Measured parameters of the FTO/glass sample.

| Measured parameter | Measured value |
|---|---|
| Thickness of glass substrate (mm) | 3.0 |
| Thickness of film (nm) | 726 |
| Surface RMS roughness (nm) | 100.5 |
| Average optical transmittance in the waveband of 380–780 nm (%) | 75.4 |
| Absorptance at the wavelength of 532 nm (%) | 4 |
| Sheet resistance (Ω/□) | 10.2 |

### 2.2. Experimental system

A diode pumped Nd:$YVO_4$ nanosecond pulsed laser (Bright Solution Ltd., Italy, Wedge532) with 532 nm wavelength was used in the experiment. The Nd:$YVO_4$ laser provided a Gaussian beam without hot-spot effects and with a pulse width of 1–2 ns, a repetition rate of 1 kHz and a maximum single pulse energy of 0.9 mJ. The beam shape/mode was $TEM_{00}$ ($M^2 < 5$), the laser output was linearly polarized with a polarization extinction ratio of 100:1 and the mean of the pulse-to-pulse stability was $\pm 2\%$. The nanosecond pulsed laser surface treatment system was composed of a beam expander, a total reflector, a vibrating mirror system (Raylaser AG, Germany, Supscan-15) and a focusing lens (with a focal length of 20 cm), as shown in Fig. 2. The laser beam diameter at the exit port was approximately 2.5 mm. The vibrating mirror system contained a focus shifter, which could adjust the focus range in the $Z$-direction from +15 mm to $-15$ mm and achieved a maximum scanning area of 40 mm × 40 mm through a computer program. The $X$–$Y$ moving stage, on which the FTO/glass sample was placed, was controlled to achieve two-dimensional motion by the computer program. The laser output energy, the scanning speed and path on the FTO film surfaces could also be set and controlled by the computer program.

### 2.3. Experimental control

During the experiment, the location of the sample was crucial due to the following reason. When the surface of the FTO layer is at or before the laser focal point, the laser beam may be focused on the surface of the glass substrate (owing to the lower thickness of the FTO layer) or inside the glass substrate (owing to the higher transparency of the glass substrate), resulting in a non-ideal treatment effect. Therefore, the surface of the FTO layer was controlled to be after the focal point of the laser beam with a defocus amount of 0.3 mm by adjusting the focus shifter in the vibrating mirror system. Then the average spot size irradiated on the film surface was about 100 μm. The scanning path of the laser was set to be back and forth along the *X*-axis, as shown in Fig. 3. The dimensions of scan area and line-scan spacing were 10 mm × 10 mm and 40 μm, respectively. Two groups of samples A and B were prepared to undergo laser irradiation with various laser fluences (*F*) and scanning speeds (*v*), see Table 2.

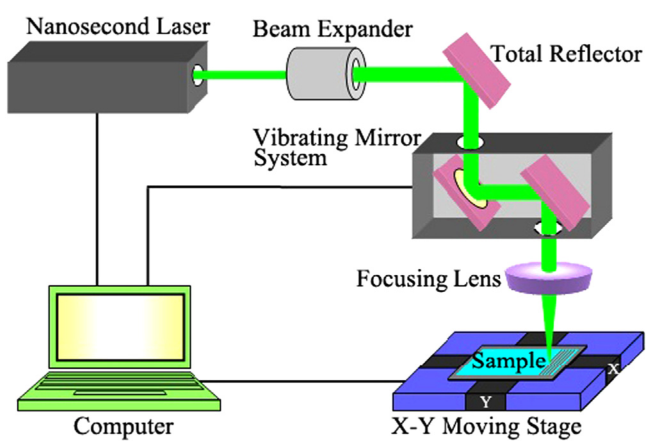


Fig. 2. Schematic diagram of the nanosecond pulsed laser surface treatment system.

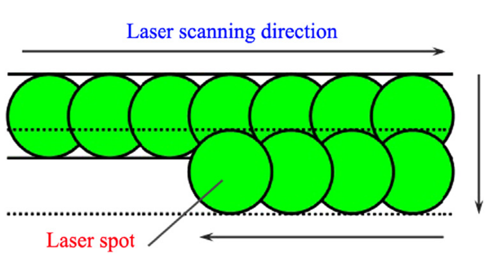


Fig. 3. Schematic diagram of the laser scanning path.

## 3. Results and discussion

### 3.1. Dependence of the crystal structures and surface morphologies of FTO/glass samples on the laser parameters

Fig. 4 shows the XRD patterns of FTO films before and after laser treatment. It is seen that the untreated FTO film only contains the $SnO_2$ tetragonal structure (JCPDS no. 41–1445) and exhibits preferred orientation along (110) plane ((1) in Fig. 4). The presence of other reflexes along (101), (200), (211), (220), (310), (301) and (321) planes indicates polycrystallinity of the film. In the case of the FTO films treated with lower *F* values or higher *v* values, the changes of all the diffraction peaks in the XRD patterns are not obvious ((2) and (5) in Fig. 4). The laser-treated film with *F* of 1.02 J/cm$^2$ and *v* of 10 mm/s shows an increase in the intensity and a decrease in the full width at half maximum (FWHM) of the (110) diffraction peak ((3) in Fig. 4), which may be due to the increase in both crystallinity and crystallite size [26]. With respect to the films treated with higher *F* values or lower *v* values, all the diffraction peaks in the XRD patterns are weakened or disappeared altogether ((4) and (6) in Fig. 4) indicating a certain

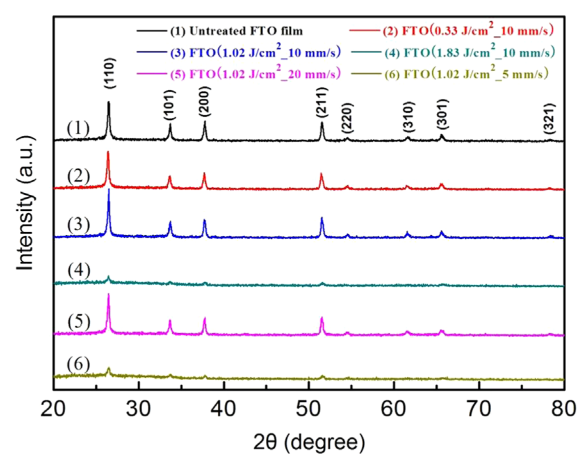


Fig. 4. XRD patterns of the untreated and the laser-treated FTO films.

Table 2
Laser parameters and optical properties of the two groups of samples

| Group number | Laser fluence, *F* (J/cm$^2$) | Scanning speed, *v* (mm/s) | Average transmittance in the waveband of 380–780 nm (%) | Absorptance at the wavelength of 532 nm (%) |
|---|---|---|---|---|
| A | 0.33 | 10 | 77.5 | 2.4 |
| | 1.02 | | 82.7 | 1.1 |
| | 1.83 | | 71.8 | 8.4 |
| | 2.48 | | 66.1 | 16.9 |
| B | 1.02 | 5 | 67.6 | 14 |
| | | 20 | 81.3 | 1.2 |
| | | 40 | 77.2 | 3.6 |

damage to the films [22], which will be further confirmed by SEM analysis.

To assess the crystal quality of the films, the crystallite size for the (110) diffraction peak was estimated according to the Scherrer formula [27]. Fig. 5 shows the variation of the calculated crystallite sizes with laser parameters $F$ and $v$. The crystallite size of the untreated FTO film was 43.3 nm. When the values of $F$ and $v$ were 1.02 J/cm$^2$ and 10 mm/s respectively, the crystallite size achieved a maximum of 78.0 nm, suggesting that grain growth of this film was significantly greater than that of others [17]. The laser-treated films with lower $F$ values or higher $v$ values showed only small increases in crystallite size, while those with higher $F$ values or lower $v$ values exhibited greater decreases in crystallite size, consistent with the XRD results.

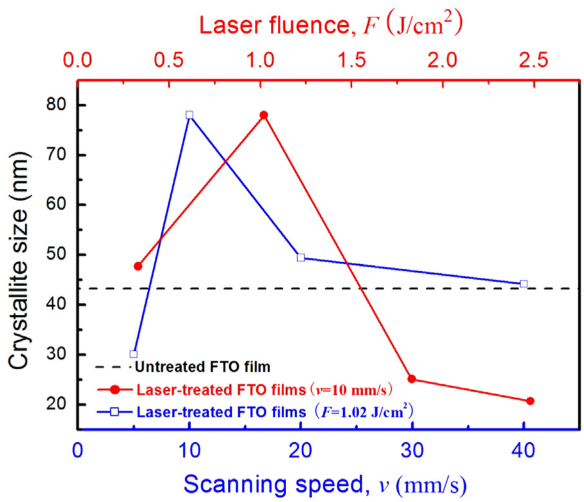


Fig. 5. Effects of laser fluence ($F$) and scanning speed ($v$) on crystallite size of the FTO films.

Fig. 6 shows the SEM images of the FTO films before and after laser treatment using a constant $v$ of 10 mm/s. The surface of the untreated FTO film shows some small and densely distributed grains (Fig. 6(a)). When the film was treated with $F$ of 0.33 J/cm$^2$, as Fig. 6(b) shows, the surface morphology involved a slight increase in the grain size and had no other apparent changes, which may be due to a gentle annealing effect caused by the lower laser fluence. As the $F$ value increased to 1.02 J/cm$^2$ shown in Fig. 6(c), the crystalline grains became greater and more uniform. It implied that the film achieved a wonderful annealing effect and a re-crystallization process had taken place in the laser-irradiated region [24]. When the film was treated with $F$ of 1.83 J/cm$^2$ or 2.48 J/cm$^2$, local regions of the film layer melted and ablated, and even the glass substrate became visible, as shown in Fig. 6(d). Obviously, the laser fluence is too high and exceeded the ablation threshold of the FTO layer of approximately 1.6 J/cm$^2$ measured in the experiment. It should also be mentioned that the surface morphologies of the films treated with a constant $F$ of 1.02 J/cm$^2$ showed a similar changing feature. That is to say that the films treated with higher (i.e. 20 mm/s and 40 mm/s) and lower (i.e. 5 mm/s) values of $v$ had the surface morphologies similar to Figs. 6(b) and (d), respectively.

Fig. 7 shows AFM images with RMS roughnesses of four sample surfaces. The RMS roughness of the untreated FTO film was 100.5 nm (Fig. 7(a)). AFM images of the surfaces of the laser-treated FTO films exhibited three kinds of surface morphologies with different RMS roughnesses. The films gently annealed with lower $F$ value (0.33 J/cm$^2$) or higher $v$ values (20 mm/s and 40 mm/s) had dense and fine-grained

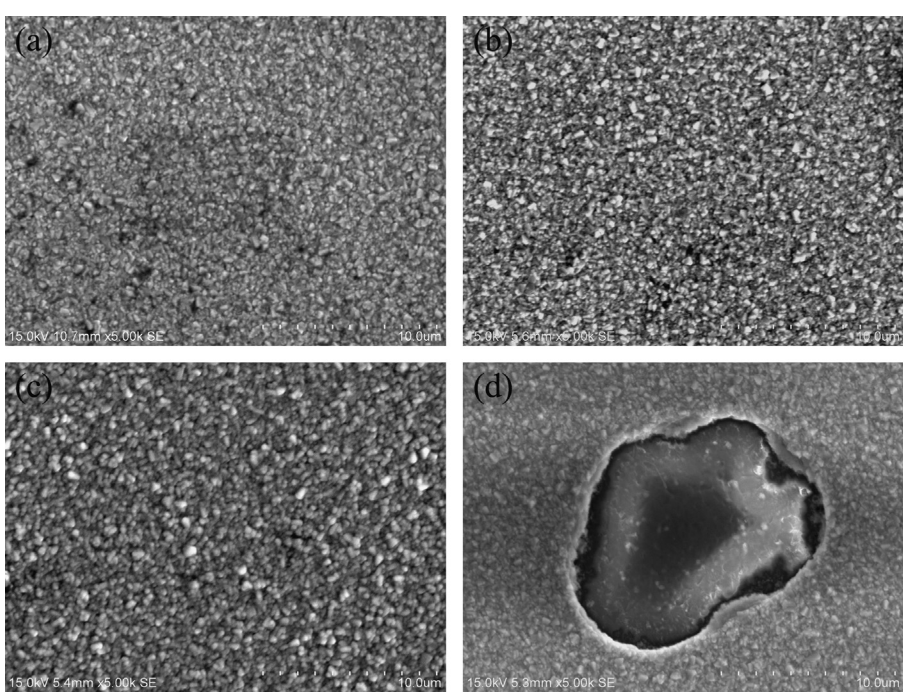


Fig. 6. SEM images of (a) the untreated FTO film and the laser-treated FTO films with $v=10$ mm/s and (b) $F=0.33$ J/cm$^2$, (c) $F=1.02$ J/cm$^2$ and (d) $F=1.83$ J/cm$^2$, respectively.

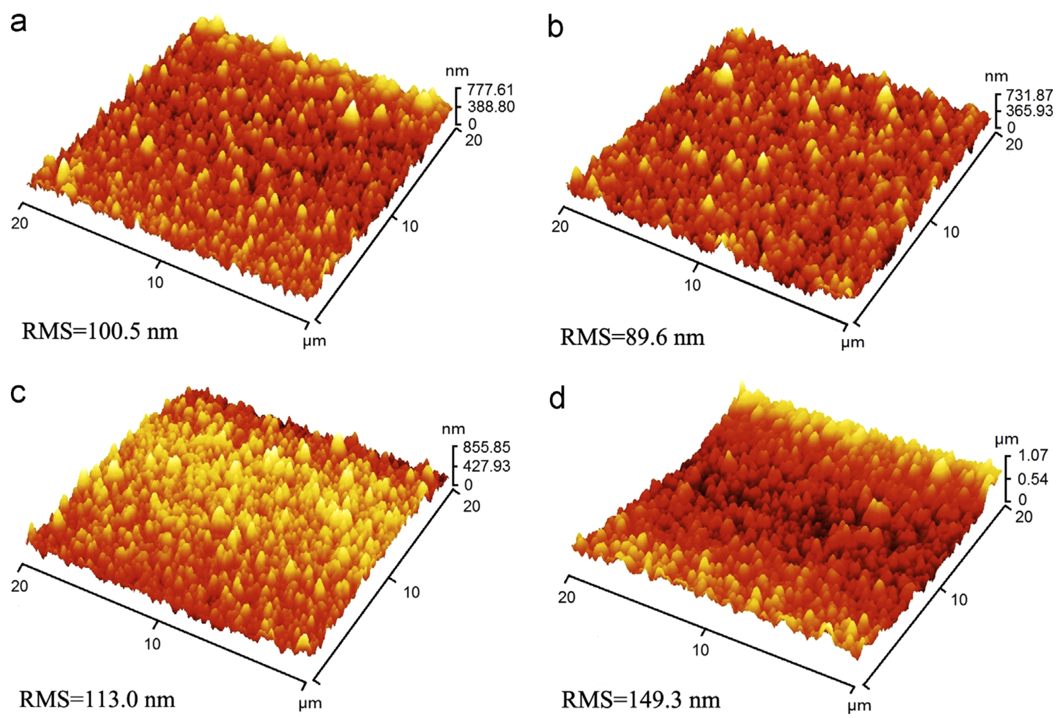


Fig. 7. AFM images of (a) the untreated FTO film and the laser-treated FTO films with $v=10$ mm/s and (b) $F=0.33$ J/cm$^2$, (c) $F=1.02$ J/cm$^2$ and (d) $F=1.83$ J/cm$^2$, respectively.

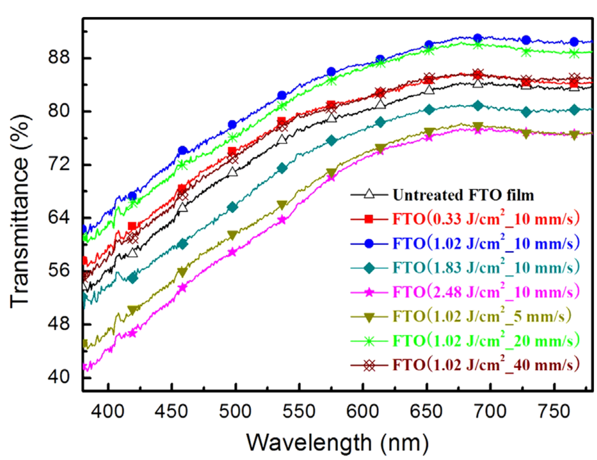


Fig. 8. Optical transmittances of the untreated and the laser-treated FTO films.

surfaces with a RMS roughness slightly lower than 100.5 nm (Fig. 7(b)). The film annealed with $F$ of 1.02 J/cm$^2$ and $v$ of 10 mm/s had an uniform and coarse-grained surface with a RMS roughness (113.0 nm) slightly greater than 100.5 nm (Fig. 7(c)), while the films partly ablated with higher $F$ values (1.83 J/cm$^2$ and 2.48 J/cm$^2$) or lower $v$ value (5 mm/s) had rugged and pit-like surfaces with a RMS roughness far greater than 100.5 nm (Fig. 7(d)). It is well known that grain size strongly influences the surface roughness of thin films [17]. The films annealed with lower $F$ values or higher $v$ values had finer and denser grains. As a result, their RMS roughness values were lower than that of both the untreated FTO film and the film annealed with $F$ of 1.02 J/cm$^2$ and $v$ of 10 mm/s.

### *3.2. Effects of the laser parameters on the photoelectric properties of FTO/glass samples*

The optical properties of the FTO films were significantly influenced by laser fluence ($F$) and scanning speed ($v$). Fig. 8 shows the optical transmittance spectra of the FTO films before and after laser treatment. The average optical transmittance in the waveband of 380–780 nm and absorptance at the wavelength of 532 nm for the laser-treated FTO films are given in Table 2. It is seen that the films treated with lower $F$ value (0.33 J/cm$^2$) or higher $v$ values (20 mm/s and 40 mm/s) had a certain increase in the average optical transmittance compared with the untreated film. The gentle annealing effect with an increase in grain size caused by laser irradiation, which brought about a loss of light scattering at grain boundaries, should be responsible for the enhancement of transmittance [28]. Meanwhile, the annealing effect could result in relatively lower extinction coefficient [29], thus reducing the absorptance at 532 nm for these films. The results shown in Fig. 8 and Table 2 also reveal that the laser-treated film with $F$ of 1.02 J/cm$^2$ and $v$ of 10 mm/s has the maximum value of average optical transmittance (82.7%) and the minimum value of absorptance (1.1%). From the SEM images at these laser parameters, the film achieved a wonderful annealing effect that resulted in greater and more uniform crystalline grains. It has been reported that the greater size and uniformity of grains could effectively reduce scattering and absorption of light in the film, which should be conducive to improving transparency of the film [30,31]. With respect to the laser-treated films of higher $F$ values (1.83 J/cm$^2$ and 2.48 J/cm$^2$) or lower $v$ value (5 mm/s), the average optical transmittance greatly decreased and the absorptance greatly increased compared with the untreated film. These could be attributed to the damage of the films [32].

The $F$ and $v$ values were also crucial to the electrical properties of the FTO films. The sheet resistance of the FTO films as functions of $F$ and $v$ is shown in Fig. 9. The film treated with $F$ of 1.02 J/cm$^2$ and $v$ of 10 mm/s had the minimum sheet resistance of 8.8 Ω/□, which was lower than that of the untreated film (10.2 Ω/□). With regard to the films treated with $F$ of 0.33 J/cm$^2$ and $v$ of 10 mm/s, the sheet resistance had an imperceptible drop compared with the untreated film. Similarly, the sheet resistances of the films treated using a constant $F$ of 1.02 J/cm$^2$ and higher $v$ values (20 mm/s and 40 mm/s) reduced to values slightly lower than that of the untreated film and remained steady. Based on the correlative analyses that have been reported, the following can be concluded. No matter what laser parameters are adopted, appropriate annealing can release internal stress and eliminate parts of the crystal defects in the films [24,33]. Furthermore, the annealing effect can also increase the grain size and distance between two neighboring grain boundaries [25]. As a result, the potential barrier height of the grain boundaries and the number of bound electrons decrease, thus enhanced mobility and reduced scattering of the carriers are achieved [18,34]. All these changes lead to the improvement of conductivity of the films. However, due to the damage caused by the laser, the sheet resistances of the films treated with higher $F$ (1.83 J/cm$^2$ and 2.48 J/cm$^2$) or lower $v$ (5 mm/s) were greatly higher than that of the untreated film [24]. In addition, the intense laser ablation could cause a certain decrease in the thickness of the films [25,35], which may also be responsible for the increase in sheet resistances.

To evaluate the overall quality of the FTO films, we estimated the figure of merit, $\varphi_{TC}$, which was defined by Haacke [36] as

$$\varphi_{TC} = T^{10}/R_s, \tag{1}$$

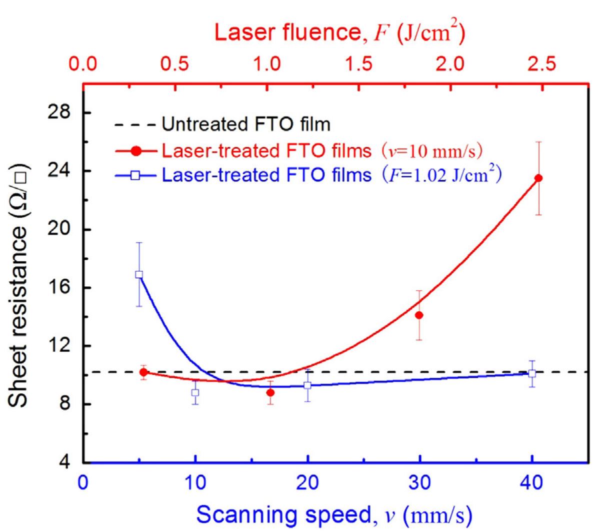


Fig. 9. Effects of laser fluence ($F$) and scanning speed ($v$) on sheet resistance of the FTO films.

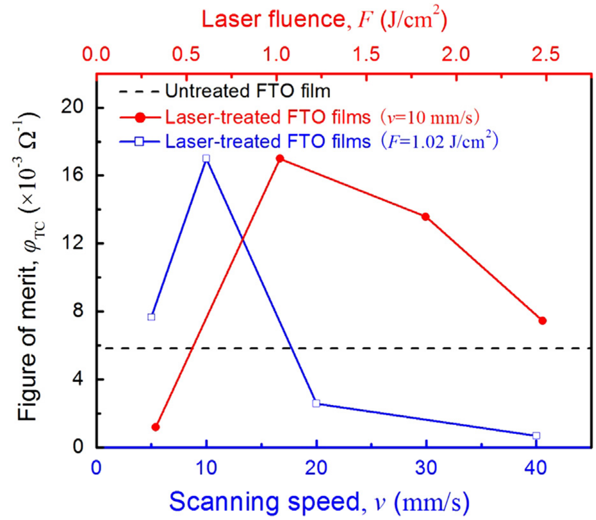


Fig. 10. Figure of merit ($\varphi_{TC}$) for the FTO films as functions of laser fluence ($F$) and scanning speed ($v$).

where $T$ and $R_s$ are the average optical transmittance in the waveband of 380–780 nm and the sheet resistance of a film, respectively. Higher values of the figure of merit represent better performance of the films [37]. Fig. 10 shows the figure of merit ($\varphi_{TC}$) for the FTO films as functions of the laser parameters ($F$ and $v$). It is obvious that the figure of merit for the laser-treated film with $F$ of 1.02 J/cm$^2$ and $v$ of 10 mm/s increases from the value of $5.82 \times 10^{-3}\ \Omega^{-1}$ for the untreated film to the maximum value of $17.00 \times 10^{-3}\ \Omega^{-1}$, indicating that the annealing effect achieved by the nanosecond laser can improve the FTO-film overall quality.

## 4. Conclusion

In summary, commercial FTO films deposited on glass substrates were irradiated with a 532 nm nanosecond pulsed laser. The effects of laser fluence and scanning speed on the surface morphology, optical and electrical properties of the FTO films were investigated. In the present study, the film treated with a laser fluence of 1.02 J/cm$^2$ and a scanning speed of 10 mm/s achieved the optimum laser annealing effect. The film had an obvious increase in crystallite size and a RMS roughness of 113.0 nm. The average optical transmittance in the waveband of 380–780 nm, the sheet resistance and the figure of merit of the film were 82.7%, 8.8 Ω/□ and $17.00 \times 10^{-3}\ \Omega^{-1}$ respectively, indicating that the photoelectric property and overall quality of the film were significantly improved. When the laser fluence was too high or the scanning speed was too low, the irradiated FTO films melted and ablated resulting in remarkable degradation of the photoelectric properties.

## Acknowledgments

This research was supported by Young's Natural Science Foundation of Jiangsu University (Grant no. JDQ03008), the National Key Basic Research Development Program of China (973 Program, Grant no. 2011CB013000), the Senior Talent

Research Foundation of Jiangsu University (Grant no. 13JDG045), the Open Research Fund Program of Jiangsu Provincial Key Laboratory of Center for Photon Manufacturing Science and Technology and a Project Funded by the Priority Academic Program Development of Jiangsu Higher Education Institutions.

## References

[1] Z. Tachan, S. Rühle, A. Zaban, Dye-sensitized solar tubes: a new solar cell design for efficient current collection and improved cell sealing, Solar Energy Materials and Solar Cells 94 (2010) 317–322.

[2] C. Sima, C. Grigoriu, S. Antohe, Comparison of the dye-sensitized solar cells performances based on transparent conductive ITO and FTO, Thin Solid Films 519 (2010) 595–597.

[3] S. Klein, M. Rohde, S. Buschbaum, D. Severin, Throughput optimized a-Si/μc-Si tandem solar cells on sputter-etched ZnO substrates, Solar Energy Materials and Solar Cells 98 (2012) 363–369.

[4] M. Chen, Z.L. Pei, C. Sun, J. Gong, R.F. Huang, L.S. Wen, ZAO: an attractive potential substitute for ITO in flat display panels, Materials Science and Engineering B 85 (2001) 212–217.

[5] S.F. Tseng, W.T. Hsiao, K.C. Huang, D. Chiang, M.F. Chen, C.P. Chou, Laser scribing of indium tin oxide (ITO) thin films deposited on various substrates for touch panels, Applied Surface Science 257 (2010) 1487–1494.

[6] A.G. Macedo, E.A. de Vasconcelos, R. Valaski, F. Muchenski, E.F. da Silva Jr., A.F. da Silva, L.S. Roman, Enhanced lifetime in porous silicon light-emitting diodes with fluorine doped tin oxide electrodes, Thin Solid Films 517 (2008) 870–873.

[7] S.J. Kim, P.S. Cho, J.H. Lee, C.Y. Kang, J.S. Kim, S.J. Yoon, Preparation of multi-compositional gas sensing films by combinatorial solution deposition, Ceramics International 34 (2008) 827–831.

[8] B.G. Lewis, D.C. Paine, Applications and processing of transparent conducing oxides, MRS Bulletin 25 (2000) 22–27.

[9] B.H. Liao, C.C. Kuo, P.J. Chen, C.C. Lee, Fluorine-doped tin oxide films grown by pulsed direct current magnetron sputtering with an Sn target, Applied Optics 50 (2011) C106–C110.

[10] K.S. Ramaiah, V.S. Raja, Structural and electrical properties of fluorine doped tin oxide films prepared by spray-pyrolysis technique, Applied Surface Science 253 (2006) 1451–1458.

[11] J.K. Yang, W.C. Liu, L.Z. Dong, Y.X. Li, C. Li, H.L. Zhao, Studies on the structural and electrical properties of F-doped $SnO_2$ film prepared by APCVD, Applied Surface Science 257 (2011) 10499–10502.

[12] L. Ding, M. Boccard, G. Bugnon, M. Benkhaira, S. Nicolay, M. Despeisse, F. Meillaud, C. Ballif, Highly transparent ZnO bilayers by LP-MOCVD as front electrodes for thin-film micromorph silicon solar cells, Solar Energy Materials and Solar Cells 98 (2012) 331–336.

[13] C. Luangchaisri, S. Dumrongrattana, P. Rakkwamsuk, Effect of heat treatment on electrical properties of fluorine doped tin dioxide films prepared by ultrasonic spray pyrolysis technique, Procedia Engineering 32 (2012) 663–669.

[14] M. Oane, F. Scarlat, S.L. Tsao, I.N. Mihailescu, Thermal fields in laser-multi-layer structures interaction, Optics and Laser Technology 39 (2007) 796–799.

[15] R.J. Winfield, L.H.K. Koh, S. O'Brien, G.M. Crean, Excimer laser processing of ZnO thin films prepared by the sol–gel process, Applied Surface Science 254 (2007) 855–858.

[16] K. Kim, S. Kim, S.Y. Lee, Effect of excimer laser annealing on the properties of ZnO thin film prepared by sol–gel method, Current Applied Physics 12 (2012) 585–588.

[17] C.Y. Tsayn, M.C. Wang, Structural and optical studies on sol–gel derived ZnO thin films by excimer laser annealing, Ceramics International 39 (2013) 469–474.

[18] S. Lee, J. Seong, D.Y. Kim, Effects of laser-annealing using a KrF excimer laser on the surface, structural, optical, and electrical properties of AlZnO thin films, Journal of the Korean Physical Society 56 (2010) 782–786.

[19] E.V. Johnson, P. Prod'homme, C. Boniface, K. Huet, T. Emeraud, P. Rocai Cabarrocas, Excimer laser annealing and chemical texturing of ZnO:Al sputtered at room temperature for photovoltaic applications, Solar Energy Materials and Solar Cells 95 (2011) 2823–2830.

[20] Q. Xu, R.D. Hong, H.L. Huang, Z.F. Zhang, M.K. Zhang, X.P. Chen, Z.Y. Wu, Laser annealing effect on optical and electrical properties of Al doped ZnO films, Optics and Laser Technology 45 (2013) 513–517.

[21] M.F. Chen, K. Lin, Y.S. Ho, Laser annealing process of ITO thin films using beam shaping technology, Optics and Lasers in Engineering 50 (2012) 491–495.

[22] C.J. Lee, H.K. Lin, C.H. Li, L.X. Chen, C.C. Lee, C.W. Wu, J.C. Huang, A study on electric properties for pulse laser annealing of ITO film after wet etching, Thin Solid Films 522 (2012) 330–335.

[23] M.Y. Pu, J.Z. Chen, I.C. Cheng, KrF excimer laser irradiated nanoporous $TiO_2$ layers for dye-sensitized solar cells: influence of laser power density, Ceramics International 39 (2013) 6183–6188.

[24] M.F. Chen, K. Lin, Y.S. Ho, Effects of laser-induced recovery process on conductive property of $SnO_2$:F thin films, Materials Science and Engineering B 176 (2011) 127–131.

[25] S.F. Tseng, W.T. Hsiao, D. Chiang, K.C. Huang, C.P. Chou, Mechanical and optoelectric properties of post-annealed fluorine-doped tin oxide films by ultraviolet laser irradiation, Applied Surface Science 257 (2011) 7204–7209.

[26] M.S. Kim, D.Y. Kim, M.Y. Cho, G. Nam, S. Kim, D.Y. Lee, S.O. Kim, J.Y. Leem, Effects of buffer layer thickness on properties of ZnO thin films grown on porous silicon by plasma-assisted molecular beam epitaxy, Vacuum 86 (2012) 1373–1379.

[27] H. Gomez, A. Maldonado, M.L. Acosta, D.R. Acosta, Gallium-doped ZnO thin films deposited by chemical spray, Solar Energy Materials and Solar Cells 87 (2005) 107–116.

[28] L.W. Wang, L.J. Meng, V. Teixeira, S.G. Song, Z. Xu, X.R. Xu, Structure and optical properties of ZnO:V thin films with different doping concentrations, Thin Solid Films 517 (2009) 3721–3725.

[29] O. Lupan, T. Pauporté, L. Chow, B. Viana, F. Pellé, L.K. Ono, B. Roldan Cuenya, H. Heinrich, Effects of annealing on properties of ZnO thin films prepared by electrochemical deposition in chloride medium, Applied Surface Science 256 (2010) 1895–1907.

[30] B.R. Kumar, T.S. Rao, Microstructural, electrical and optical properties of DC reactive magnetron sputtered zinc aluminum oxide thin films for optoelectronic devices, Journal of Optoelectronics and Biomedical Materials 4 (2012) 35–42.

[31] M. Hezam, N. Tabet, A. Mekki, Synthesis and characterization of DC magnetron sputtered ZnO thin films under high working pressures, Thin Solid Films 518 (2010) 161–164.

[32] W. Chung, M.O. Thompson, P. Wickboldt, D. Toet, P.G. Carey, Room temperature indium tin oxide by XeCl excimer laser annealing for flexible display, Thin Solid Films 460 (2004) 291–294.

[33] Z. Jiang, X.K. Chen, Stress release and control of thin films materials used in devices fabrication, Chinese Journal of Vacuum Science and Technology 28 (2008) 17–21.

[34] E. Shanthi, V. Dutta, A. Banerjee, K.L. Chopra, Electrical and optical properties of undoped and antimony-doped tin oxide films, Journal of Applied Physics 51 (1980) 6243–6251.

[35] M.H. Badawi, B.J. Sealy, K.G. Stephens, Vaporisation of GaAs during laser annealing, Electronics Letters 15 (1979) 786–787.

[36] G. Haacke, New figure of merit for transparent conductors, Journal of Applied Physics 47 (1976) 4086–4089.

[37] M.C. Jun, J.H. Koh, Effects of NIR annealing on the characteristics of Al-doped ZnO thin films prepared by RF sputtering, Nanoscale Research Letters 7 (2012) 294–300.